

Very Extended Shapes in the $A \sim 110$ Region

R. M. Clark,¹ P. Fallon,¹ A. Gorgen,¹ M. Cromaz,¹ M. A. Deleplanque,¹ R. M. Diamond,¹ G. J. Lane,^{1,*} I. Y. Lee,¹
 A. O. Macchiavelli,¹ R. G. Ramos,¹ F. S. Stephens,¹ C. E. Svensson,^{1,†} K. Vetter,¹ D. Ward,¹ M. P. Carpenter,²
 R. V. F. Janssens,² and R. Wadsworth³

¹*Nuclear Science Division, Lawrence Berkeley National Laboratory, Berkeley, California 94720*

²*Physics Division, Argonne National Laboratory, Argonne, Illinois 60439*

³*Department of Physics, University of York, Heslington, York, YO1 5DD United Kingdom*

(Received 29 May 2001; published 29 October 2001)

High-angular-momentum states in ^{108}Cd were populated via the $^{64}\text{Ni}(^{48}\text{Ca}, 4n)$ reaction at a beam energy of 207 MeV. Gamma rays were detected using the Gammasphere array. A rotational band has been observed with a dynamic moment of inertia and deduced lower limit of the quadrupole moment suggesting a major-to-minor axis ratio larger than 1.8:1, placing it among the most deformed structures identified in any nucleus, to date.

DOI: 10.1103/PhysRevLett.87.202502

PACS numbers: 21.10.Re, 23.20.Lv, 27.60.+j

Within the framework of the nuclear harmonic-oscillator model, one expects the existence of favorable shell gaps that appear regularly as a function of deformation and nucleon number. They are predicted to occur for particular magic numbers and at deformations corresponding to integer ratios of the lengths of the major-to-minor axes (e.g., for superdeformed (SD) nuclei, with a quadrupole deformation of $\epsilon_2 = 0.6$, the ratio is 2:1). While more realistic nuclear potentials alter these simple regularities, SD structures [1] with nearly a 2:1 axis ratio have been found in nuclei of the $A \approx 150$ (close to ^{152}Dy) and $A \approx 240$ (close to ^{236}U) mass regions and, most recently, in ^{91}Tc . In the $A \sim 190$ region the SD structures have a smaller axis ratio of $\sim 1.7:1$. Mass regions near $A \sim 130, 80, 60,$ and 40 have also been described as regions of SD nuclei.

Many of the models that explain SD nuclei predict additional minima in the potential energy surfaces at even larger deformations that correspond to prolate shapes with major-to-minor axis ratios of about 3:1. These are the long-sought-for hyperdeformed nuclei, and they are generally predicted to become yrast (the state with the lowest energy for a particular angular momentum is called the "yrast" state) at very high angular momentum (e.g., $\approx 80\hbar$ in ^{152}Dy [2]). It is questionable whether hyperdeformed structures can survive fission since the corresponding barriers tend to be very small at these high-angular-momentum values. Observation of hyperdeformation would have a profound impact on our understanding of fission barriers and shape parametrizations, and provide a stringent test of theoretical models.

Calculations by Werner and Dudek [3] for a wide range of nuclei attempted to predict likely regions of super- and hyperdeformation. A stable secondary minimum at large deformation ($\epsilon_2 \approx 0.65$) was found for ^{108}Cd at an angular momentum about $60\hbar$. Also, recent calculations by Chasman [4], using a cranked Strutinsky method and a four-dimensional shape space representing quadrupole,

octupole, hexadecapole, and necking degrees of freedom, predict that a region of shape minima at deformations with 2:1 axis ratios (or larger) exists at high angular momentum in nuclei with $A \sim 110$. In fact, the calculations find that many nuclei have minima in the potential energy surfaces corresponding to a variety of extended nuclear shapes. The calculated fission barriers are small at the angular momenta at which these shapes become yrast (typically $\approx 60\hbar$) making it very unlikely that the shapes can be observed experimentally. However, notable exceptions are also found. In particular, very extended shapes, stable against fission, are predicted for ^{106}Cd ($Z = 48, N = 58$) and ^{108}Cd ($Z = 48, N = 60$). For ^{108}Cd the calculations predict a minimum in the potential energy surface corresponding to a shape with an axis ratio of $\approx 2.3:1$ which becomes yrast at $I \approx 60\hbar$. The very extended shape minimum results from a large shell correction for both protons and neutrons at this deformation, which lies intermediate between super- and hyperdeformation. Moreover, at this deformation the $h_{11/2}$ proton and $i_{13/2}$ neutron orbitals lie at the Fermi surface. These are the intruder states normally associated with superdeformation in the $A \sim 130$ region, and may be regarded as superintruder levels for configurations in the Cd nuclei. For ^{108}Cd , the outer barrier to fission is calculated to be >9 MeV at $I = 60\hbar$ and >6 MeV at $70\hbar$, implying that the nucleus at this deformation is stable against fission and that it should be possible to observe the discrete gamma-ray decay of states in this minimum over a range of angular momentum.

Motivated by such considerations we performed an experiment to search for very deformed shapes in ^{108}Cd . High-angular-momentum states in ^{108}Cd were populated in the $^{64}\text{Ni}(^{48}\text{Ca}, 4n)$ reaction with a beam energy of 207 MeV. The beam, accelerated by the ATLAS accelerator at the Argonne National Laboratory, was incident on a target comprising two stacked foils of $\approx 500 \mu\text{g}/\text{cm}^2$ ^{64}Ni . Gamma rays were detected with the Gammasphere array [5] which for this experiment comprised 101

Compton-suppressed Ge detectors. Thick Pb and Cu absorbers (≈ 0.126 cm and 0.005 cm, respectively) were placed in front of the Ge detectors to reduce the number of low-energy gamma rays that could pass the trigger conditions. A total of $\approx 1.3 \times 10^9$ coincidence events, with at least six Compton-suppressed gamma rays, was collected. The off-line analysis was helped greatly by the code BLUE [6]. The entire data set, in this case comprising the gamma-ray energies and angles of detection for all events passing through a prompt-coincidence time cut, were stored in an indexed, energy-ordered database on computer disk. This BLUE database could be queried to create gated spectra in a few minutes for any combination of chosen gates in any fold. In addition, various E_γ - E_γ matrices and an E_γ - E_γ - E_γ cube were sorted.

A sequence of mutually coincident, regularly spaced transitions was found, and a spectrum is shown in Fig. 1. The band is in coincidence with known transitions [7] of ^{108}Cd and, therefore, it is assigned to this nucleus. The intensity of the new band is estimated to be $\approx 1.4\%$ of the ^{108}Cd channel (which accounts for $\approx 15\%$ of the total fusion-evaporation cross section). Angular distribution ratios indicate that the in-band transitions are stretched quadrupoles, presumably electric-quadrupole transitions. A plot of the dynamic moment of inertia, $J^{(2)}$ (which can be related to the energy spacing of transitions, ΔE_γ , since $J^{(2)} = 4/\Delta E_\gamma [\hbar^2 \text{MeV}^{-1}]$ in the case of quadrupole transitions), is shown in Fig. 2. For comparison to structures in other mass regions we have scaled the moment of inertia by that of a rigid sphere ($J_{\text{sphere}}^{\text{rigid}} = A^{5/3}/72 [\hbar^2 \text{MeV}^{-1}]$). The rise at low rotational frequency probably indicates a change in the intrinsic configuration upon which the band is built.

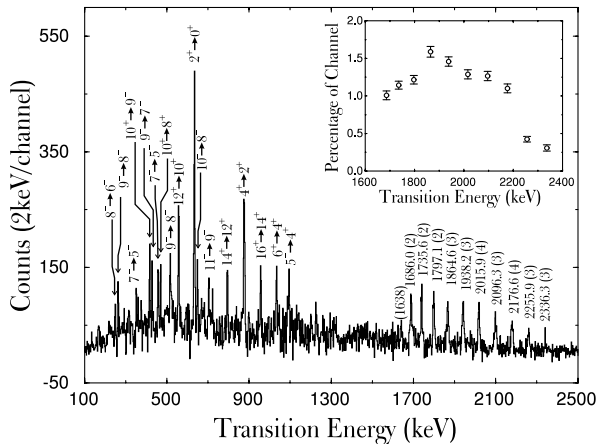


FIG. 1. Spectrum formed from a summation of all triple-gated combinations on in-band transitions for events with fold ≥ 4 . Low-lying transitions in ^{108}Cd are marked with the angular momenta and parities of the initial and final states. The in-band transitions are marked with their measured transition energies and uncertainties (in keV). The inset shows the relative intensity (as a percentage of the intensity of the ^{108}Cd channel) of the in-band transitions.

In order to estimate the angular momenta of in-band states we assume that the kinematic moment of inertia, $J^{(1)} = 2I/E_\gamma [\hbar^2 \text{MeV}^{-1}]$, is equal to $J^{(2)}$ at high angular momentum. There is no *a priori* justification for this assumption but at very high angular momentum and deformation it is probable. For example, the yrast SD band in ^{152}Dy [8], which has recently been linked to low-lying normal-deformed states [9], is known to have $J^{(1)} \approx J^{(2)}$. We estimate that the lowest state in the new band has angular momentum, $I = 40(2)\hbar$, and the highest has $I = 60(2)\hbar$. The highest angular-momentum state from which a known transition is observed in coincidence with the band is 16^+ . Thus, there is an angular-momentum region of over $20\hbar$ through which the gamma-ray flux from the band must pass but through which we have not identified a path. This may be partly due to the high fragmentation of the flux as it passes through normal-deformed states in the decay scheme [7], but such a large angular-momentum gap is unusual.

The scaled $J^{(2)}$ moment of inertia for the band in ^{108}Cd and for the yrast SD band in ^{152}Dy are plotted in Fig. 2. The values of $J^{(2)}$ are higher for the band in ^{108}Cd than those of the band in ^{152}Dy . Assuming rigid rotation ($J^{(1)} = J^{(2)} = J^{\text{rigid}}$) of a prolate ellipsoid, it is possible to estimate the deformation since

$$J^{\text{rigid}} = \frac{A^{5/3}}{72} \frac{1+x^2}{2x^{2/3}} \hbar^2 \text{MeV}^{-1}, \quad (1)$$

where x is the ratio of the major-to-minor axes. Here, we have ignored higher order shape degrees of freedom and the effects of triaxiality or necking. Figure 2 also shows the expected rigid-body moments of inertia for prolate nuclei with $x = 1, 3/2, 2,$ and 3 . Taking the average moments of inertia we find $x \approx 1.9$ for the band in ^{108}Cd (using the $J^{(2)}$ values away from the low-energy rise seen in Fig. 2) and $x \approx 1.7$ for the band in ^{152}Dy .

The moment of inertia is not always a good indicator of the deformation since it is affected by other factors such as pairing [10]. In an effort to gain a more accurate estimate of the deformation, limits on the quadrupole moment, Q_0 , can be deduced by measuring the residual Doppler shifts of transitions from states that decay while the recoil nucleus is traversing the thin target [11]. Figure 3 shows plots of the deduced fractional Doppler shifts, $F(\tau) (= \beta/\beta_0)$, where β is the average recoil velocity at which a transition is emitted and β_0 is the average initial recoil velocity after the nucleus is formed). The open triangles are the $F(\tau)$ values for transitions in the new band while the open circles are $F(\tau)$ values, obtained in this experiment, for a normal-deformed band in ^{104}Pd [12]. All the $F(\tau)$ values were deduced from analysis of double-gated spectra using the different detector angles, and the errors include systematic effects associated with different gating conditions, backgrounds, and the fitting procedure. The uncertainty in determining the initial recoil velocity, β_0 , is indicated by

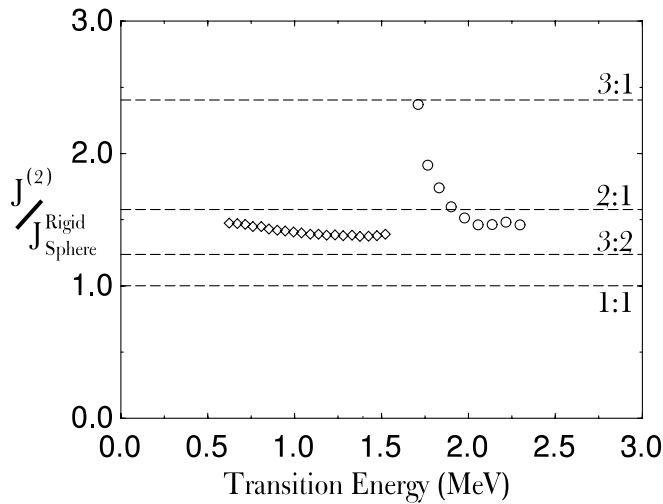


FIG. 2. Dynamic moments of inertia, $J^{(2)}$, for the new band in ^{108}Cd (circles) and the yrast SD band in ^{152}Dy (diamonds), scaled by the values for a rigid sphere. Also shown with the dashed lines are the expected values for rigid prolate ellipsoids with major-to-minor axis ratios, x , of 1, $3/2$, 2, and 3.

the horizontal dashed lines. This represents the combined systematic error assuming both a 1 MeV uncertainty in the beam energy and a 10% uncertainty in the target thickness.

For comparison, $F(\tau)$ curves were calculated using standard stopping powers [13]. Note, an additional systematic uncertainty is introduced through the choice of stopping powers. In the calculations for the new band, side-feeding

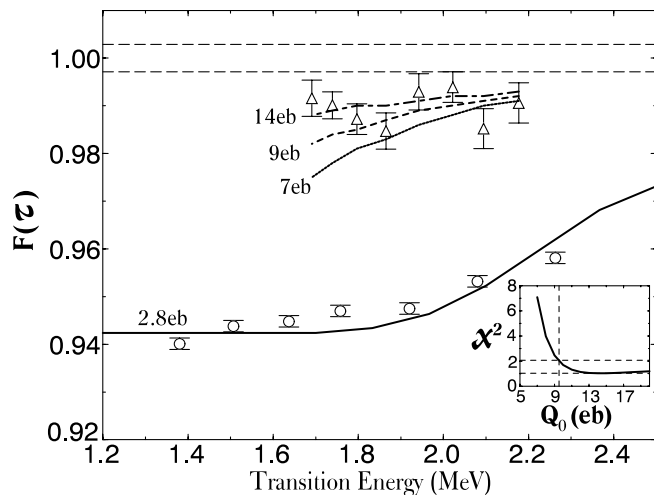


FIG. 3. Experimentally deduced $F(\tau)$ values for the new band in ^{108}Cd (triangles) and a known normally deformed band in ^{104}Pd (circles). The dashed straight lines in the upper part of the figure show the estimated uncertainty in determining the initial recoil velocity. Calculated $F(\tau)$ curves are also shown and they are labeled with the associated Q_0 value. The inset shows the reduced χ^2 for the fit of the calculated curves to the deduced values for the band in ^{108}Cd as a function of Q_0 . The dashed horizontal lines shown are for $\chi_{\min}^2 = 1.04$ and for $\chi^2 = \chi_{\min}^2 + 1$. The dashed vertical line is at the estimated lower limit for the quadrupole moment of $Q_0 = 9.5\text{eb}$.

cascades of four levels in the topmost three in-band states (see inset of Fig. 1 showing the relative intensities along the band) were assumed to have the same quadrupole moment and moment of inertia as those of the band itself. For the structure in ^{104}Pd , a recent Doppler shift attenuation measurement under near identical experimental conditions but using a Au-backed target [14], found a quadrupole moment of $Q_0 = 2.80(5)\text{eb}$. Figure 3 shows the calculated $F(\tau)$ curve for this structure assuming this value of Q_0 . The simulation for ^{104}Pd was performed under a similar set of assumptions as the simulations for the band in ^{108}Cd . The agreement with the deduced $F(\tau)$ values is extremely good for the ^{104}Pd band, adding confidence to our results for the ^{108}Cd band. Calculated $F(\tau)$ curves for this new band, assuming $Q_0 = 7, 9$, and 14eb , are shown. From fitting the χ^2 curve (shown in the inset of Fig. 3) we find $\chi_{\min}^2 = 1.04$ at $Q_0 \approx 14\text{eb}$ and a lower limit of $Q_0 = 9.5\text{eb}$ for $\chi_{\min}^2 + 1$ (shown by the dashed lines in the inset of Fig. 3). Therefore, the lower limit of the transition quadrupole moment of the new band is taken to be $Q_0 = 9.5\text{eb}$.

For a prolate ellipsoid the quadrupole moment can be related to the major-to-minor axis ratio, x , by [15]

$$Q_0 = \frac{2}{5} ZR^2 \frac{x^2 - 1}{x^{2/3}} \times 10^{-2}\text{eb}, \quad (2)$$

where $R = 1.2A^{1/3}$ fm. For the new band, this suggests that $x \geq 1.8$. For comparison Table I presents the axis ratios, estimated in this way, for suggested SD bands in ^{36}Ar [16], ^{60}Zn [17], ^{82}Sr [18], ^{91}Tc [19], ^{132}Ce [20], ^{152}Dy [21], ^{192}Hg [22], and ^{236}U [23]. It is instructive to plot the normalized quadrupole moments, $Q_0/(2/5ZR^2)$, for these nuclei and compare them to those of yrast states across the nuclear chart. Such a plot is presented in Fig. 4. The solid dots are the quadrupole moments deduced from the measured $B(E2)$ values for $2^+ \rightarrow 0^+$ transitions in even-even nuclei [24]. Shell effects can be clearly seen, such as the large drop centered around $A = 208$ corresponding to the spherical doubly magic nucleus, ^{208}Pb . The solid line shows the dependence assuming $\epsilon_2 \propto A^{-1/3}$ [25]. Several

TABLE I. The measured quadrupole moments and deduced major-to-minor axis ratios, x , for SD bands in different mass regions.

Nucleus	Q_0 (eb)	x
^{36}Ar	$1.18^{+0.09}_{-0.09}$	$1.55^{+0.04}_{-0.04}$
^{60}Zn	$2.75^{+0.45}_{-0.45}$	$1.54^{+0.10}_{-0.10}$
^{82}Sr	$3.54^{+0.15}_{-0.14}$	$1.47^{+0.02}_{-0.02}$
^{91}Tc	$8.1^{+1.9}_{-1.4}$	$1.85^{+0.21}_{-0.14}$
^{108}Cd	>9.5	>1.8
^{132}Ce	$7.4^{+0.3}_{-0.3}$	$1.45^{+0.02}_{-0.02}$
^{152}Dy	$17.5^{+0.4}_{-0.2}$	$1.85^{+0.02}_{-0.01}$
^{192}Hg	$17.7^{+0.8}_{-0.8}$	$1.61^{+0.03}_{-0.02}$
^{236}U	32^{+5}_{-5}	$1.84^{+0.14}_{-0.14}$

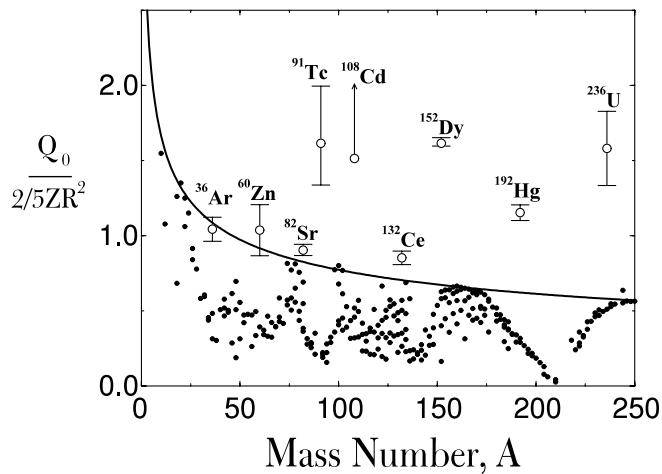


FIG. 4. Plot of normalized quadrupole moment versus mass number for ground-state (solid dots) and SD bands (open symbols) in ^{36}Ar , ^{60}Zn , ^{82}Sr , ^{91}Tc , ^{108}Cd , ^{132}Ce , ^{152}Dy , ^{192}Hg , and ^{236}U . The solid line shows the expected dependence assuming $\epsilon_2 \propto A^{-1/3}$ and is scaled to the experimental values at midshells.

of the bands summarized in Table I have large deviations from the ground-state deformations, indicating the unusual origin of these structures which reside in an isolated minimum at extreme deformation.

In summary, a rotational sequence of quadrupole transitions has been observed in ^{108}Cd . The estimated angular momenta imply that states in this band lie between $I = 40(2) - 60(2)\hbar$. The moments of inertia and the deduced lower limit of the transition quadrupole moment suggest a very extended quadrupole ellipsoidal shape of the nucleus, with a major-to-minor axis ratio, $x \geq 1.8$. This is among the most deformed structures ever observed, and it is possible that the band may have a $>2:1$ major-to-minor axis ratio as predicted by Chasman. Moreover, calculations of very extended shape minima with low predicted fission probabilities, as expected in the case of ^{108}Cd , present a considerable challenge to theory and such studies may point the way to firmer predictions of stable hyperdeformed nuclei, accessible to experimental investigation.

We express our gratitude to the crew and staff of ATLAS, and Andrzej Lipski (SUNY) for making the high-quality target foils. The help of John Greene (ANL) with the targets during the run was invaluable. Our thanks also go to Rick Firestone (LBNL) for his help in using ENSDF. This work has been supported in part by the U.S. DOE under Contracts No. DE-AC03-76SF00098 (LBNL) and No. W-31-109-ENG-38 (ANL). Two of us

(R. M. C. and R. W.) would like to acknowledge partial support from NATO under Grant No. CRG 972142.

*Present address: Department of Nuclear Physics, The Australian National University, Canberra ACT 0200, Australia.

†Present address: Department of Physics, University of Guelph, Guelph, Ontario, N1G 2W1, Canada.

- [1] B. Singh, R. B. Firestone, and S. Y. Chu, Lawrence Berkeley Laboratory, Report No. LBL-38004, 1997.
- [2] J. Dudek, T. Werner, and L. L. Riedinger, Phys. Lett. B **211**, 252 (1988).
- [3] T. Werner and J. Dudek, At. Data Nucl. Data Tables **59**, 1 (1995).
- [4] R. R. Chasman, Argonne National Laboratory Preprint PHY-9018-TH-98, 1998 (to be published); Phys. Rev. C **64**, 024311 (2001).
- [5] I. Y. Lee, Nucl. Phys. **A520**, 641c (1990).
- [6] M. Cromaz *et al.*, Nucl. Instrum. Methods Phys. Res., Sect. A **462**, 519 (2001).
- [7] N. S. Kelsall *et al.*, Phys. Rev. C **61**, 011301(R) (2000); I. Thorslund *et al.*, Nucl. Phys. **A564**, 285 (1993).
- [8] P. J. Twin *et al.*, Phys. Rev. Lett. **57**, 811 (1986).
- [9] T. Lauritsen *et al.* (to be published).
- [10] S. T. Belyaev, Mat.-Fys. Medd. K. Dan. Vidensk. Selsk. **31**, No. 11 (1959).
- [11] B. Cederwall *et al.*, Nucl. Instrum. Methods Phys. Res., Sect. A **354**, 591 (1995).
- [12] A. O. Macchiavelli *et al.*, Phys. Rev. C **38**, 1088 (1988).
- [13] J. F. Ziegler, J. P. Biersack, and U. Littmark, *The Stopping and Ranges of Ions in Matter* (Pergamon, London, 1985), Vol. 1.
- [14] R. G. Ramos *et al.* (to be published).
- [15] L. D. Landau, E. M. Lifshitz, and L. P. Pitaevskii, in *Electrodynamics of Continuous Media*, Landau and Lifshitz Course of Theoretical Physics, Vol. 8 (Pergamon, New York, 1984), 2nd ed., p. 25.
- [16] C. E. Svensson *et al.*, Phys. Rev. C **63**, 061301(R) (2001).
- [17] C. E. Svensson *et al.*, Phys. Rev. Lett. **82**, 3400 (1999).
- [18] F. Lerma *et al.*, Phys. Rev. Lett. **83**, 5447 (1999).
- [19] E. Ideguchi *et al.*, Phys. Lett. B **492**, 245 (2000).
- [20] R. M. Clark *et al.*, Phys. Rev. Lett. **76**, 3510 (1996).
- [21] D. Nisius *et al.*, Phys. Lett. B **392**, 18 (1997).
- [22] E. F. Moore *et al.*, Phys. Rev. C **55**, R2150 (1997).
- [23] V. Metag, D. Habs, and H. J. Specht, Phys. Rep. **65**, 1 (1980).
- [24] Evaluated Nuclear Structure Data File (ENSDF), a database maintained by the National Nuclear Data Center, Brookhaven National Laboratory.
- [25] A. Bohr and B. R. Mottelson, *Nuclear Structure* (Benjamin, New York, 1969/1975), Vol. 2, p. 49.